ACS APPLIED MATERIALS & INTERFACES

www.acsami.org

Research Article

3D Multiscale Micro-/Nanofolds by Femtosecond Laser Intermittent Ablation and Constrained Heating on a Shape Memory Polymer

Cheng Xue, Yachao Zhang, Longfu Li, Yanlei Hu, Chao Chen, Yuegan Song, Hongshu You, Rui Li, Jiawen Li,* Dong Wu,* and Jiaru Chu

Cite This: *ACS Appl. Mater. Interfaces* 2021, 13, 23210–23219

Read Online

ACCESS | Metrics & More | Article Recommendations | Supporting Information

ABSTRACT: Spontaneous wrinkling of films with a thickness gradient offers a new opportunity for constructing various 3D hierarchical surface morphologies. Unfortunately, accurately and facilely controlling the gradient film thickness to yield multiscale and 3D hierarchical micro-/nanostructures is still difficult. Here, a rapid, facile, and highly controllable fabricating strategy for realizing 3D multiscale hierarchical micro-/nanofolds on a shape memory polymer (SMP) surface is reported. First, the nanoparticle film with gradient thickness is rapidly (100 ms to 4 s) and facilely obtained by laser intermittent ablation on the SMP, termed as laser ablation-induced gradient thickness film. Following one-time constrained heating, the 3D micropillars grow out of the substrate based on the "self-growing effect," and the nanoparticle gradient film on its top shrinks into multiscale micro-/nanofolds simultaneously. Significantly, the evolution process and the underlying mechanism of the 3D micro-/nanofolds are systematically investigated. Fundamental basis enables us to accurately regulate the gradient thickness of nanoparticle films and feature size of folds by varying laser scanning times and scanning path. Finally, desirable patterns on micro-/nanofolds can be readily realized by programmable laser cleaning technology, and the tunable adhesion of the water droplet on the multiscale structured surface is demonstrated, which is promising for microdroplet manipulation.

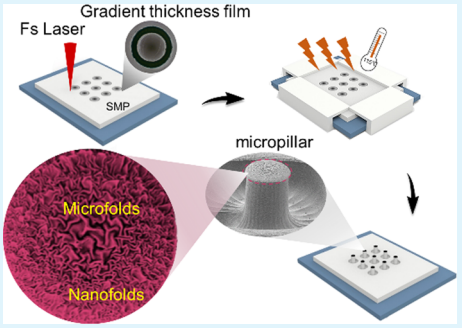

KEYWORDS: *thickness gradient, shape memory polymer, femtosecond laser, 3D multiscale micro/nano folds, polymer self-growth*

1. INTRODUCTION

Creatures in nature have evolved a variety of intriguing features and functionalities closely correlated with their intrinsic micro-/nanostructures. For example, the multiscale structures composed of submicron keratin hairs and nanoscaled spatulae on gecko feet have been mimicked for reversible adhesive properties,[1,2] the hierarchical structures consisting of cell papillae and wax nanocrystals on the surface of lotus leaves have been applied to self-cleaning surfaces,[3−5] and the structures of the mosquito eye composed of hundreds of microscale hemispheres that are covered with nanoscale nipples have been employed to antifogging properties.[6,7] Reproducing these 3D multiscale hierarchical micro-/nanoscale patterns leads to admirable opportunities for both the academic research and practical usage.[8−13] Surface wrinkling has been proven to be a powerful tool for preparing 3D multiscale micro-/nanostructures.[14−19] Based on a rigid/soft bilayer system with a rigid film resting on a compliant foundation, compressive strain is yielded on the skin layer by releasing the prestrained substrate;[19−25] thus, various 3D micro-/nanowrinkles will be induced by surface instability.

In regard to the rigid film, metal sputtering,[26−28] chemical vapor deposition[29,30] and polymer polymerization[31,32] are usually employed to selectively deposit a thin layer on the substrate or modify the top skin layer of the substrate with external stimuli such as plasma,[33−35] reactive ion etching,[36−38] and ultraviolet ozone.[39,40] To achieve 3D micro-/nanowrinkles, the prestrained substrate like micropillars,[18,41] microcones,[42] or curved surfaces[19,23,43,44] (e.g., microspheres,[28] fibers,[30] and tubes[29]) are desired to be prepared in advance, which inevitably requires multistep experimental operations. Furthermore, those otherwise promising methods suffer from a major drawback: the prepared film has a uniform thickness, which makes it difficult to achieve multiscale wrinkles upon single strain release.

Efforts have been devoted to realize the multiscale wrinkles by preparing a gradient thickness film (GTF). Stafford et al.[21,45,46] reported a novel flow coating method to prepare the GTF by controlling the sliding speed of the flat blade to draw a toluene solution of polystyrene (PS) across a Si surface and then transferring the GTF to another flexible substrate for generating multiscale wrinkles. Tan et al.[47] presented a dip-coating approach to prepare the GTF by adjusting the

Received: March 5, 2021
Accepted: April 29, 2021
Published: May 7, 2021

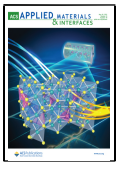

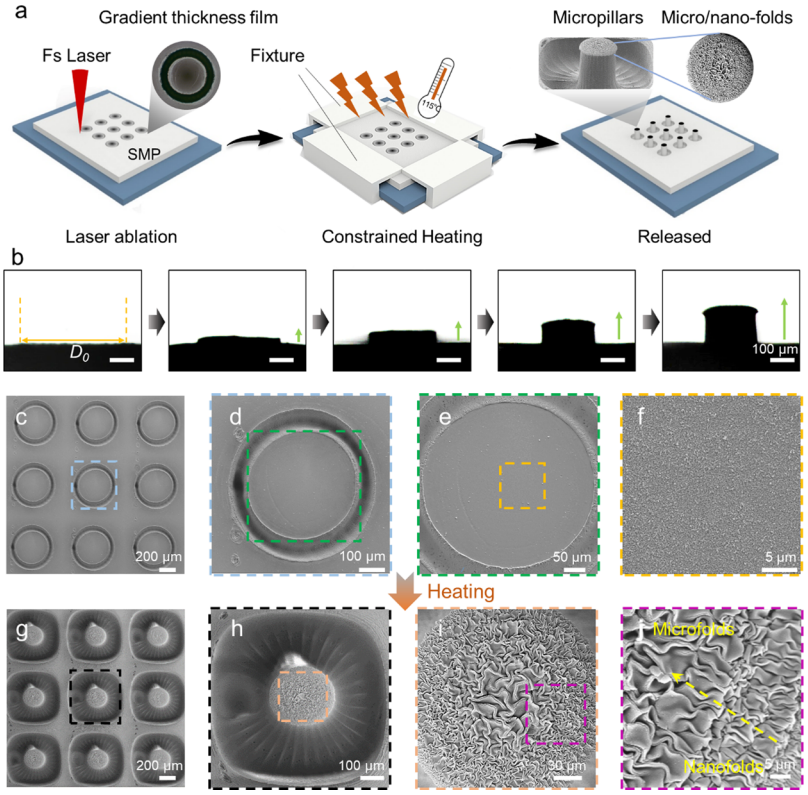

Figure 1. Preparation of the GTF and multiscale micro-/nanofolds on the micropillars by an accurate and rapid laser ablation-induced GTF-forming method and one-time constrained heating. (a) Schematic diagram of the fabrication process. The left inset is the optical image of the nanoparticle GTF. The right insets are the SEM images of the micropillar and the micro-/nanofolds. (b) Optical images showing the growth of pillars as the heating time increases. (c–f) Enlarged view of SEM images of the nanoparticle GTF fabricated by the femtosecond laser intermittent ablation on the SMP. (g–j) Enlarged view of SEM images of the formed micro-/nanofolds on the micropillar in (b) by constrained heating. The yellow arrow indicates that the width of the folds gradually increases from the nanosize to microsize in the radial direction.

concentration of graphene oxide droplets, and then the gradient folds were generated by slowly releasing the air from the inflated latex balloon. Ni et al.[48] proposed a selective deposition method to prepare the GTF by regulating the distance between the high temperature-induced prestrained polydimethylsiloxane and shutter; after cooling, the multiscale directional wrinkles were prepared. However, these methods suffer from inaccurate gradient thickness control of films or time-consuming (preparing GTF for dozens of minutes to several hours) or multistep operations. In this regard, seeking an accurate, rapid, and facile GTF-forming method for preparing 3D multiscale wrinkles is still a timely challenge.

Herein, by combining the superior deformability of shape memory polymer (SMP) and intermittent laser processing technology, a rapid, facile, and highly controllable fabricating method for realizing 3D multiscale hierarchical micro-/nanofolds is reported. First, the nanoparticle film with gradient thickness is easily and quickly (100 ms–4 s; the efficiency is increased by at least 100 times) obtained via laser intermittent ablation on the SMP. Following one-time constrained heating, the 3D micropillars grow out of the substrate based on the "self-growing effect,"[49] and the nanoparticle GTF on its top shrinks into multiscale micro-/nanofolds simultaneously. To further capture the physics of the process, the evolution of the 3D multiscale micro-/nanofolds is systematically investigated, and the quantitative relationship among the sizes of micropillar and the heating time, the feature size of folds and the heating time, and the thickness of the GTF and scanning times are revealed. On this basis, by adjusting laser scanning times and scanning path, a controllable feature size of micro-/nanofolds and the thickness of the GTF are readily realized. In addition, by taking advantage of the programmable laser cleaning technology,[50,51] the desirable micro-/nanofold pattern is achieved. This method is noncontact and template-free. Last but not least, the structured surfaces with tunable adhesion to the water droplet is demonstrated, which is promising for microdroplet manipulation.

2. RESULTS AND DISCUSSION

2.1. Preparation of the GTF and 3D Multiscale Micro-/Nanofolds Using Femtosecond Laser Intermittent Ablation and Constrained Heating. The fabrication process of 3D multiscale micro-/nanofolds is depicted in Figure 1a. The SMP we used is a heat-shrinkable thermoplastic PS film.[27,49] First, the laser spot is focused on the surface of a thermal-shrinkable SMP and intermittently scanned along a circle for certain times, and then, the nanoparticles would be induced by laser ablation and deposited inside the circle. According to the energy-dispersive spectroscopy (EDS), Fourier transform infrared spectroscopy (FT-IR), and X-ray photoelectron spectroscopy (XPS) analyses of the nanoparticles, it can be concluded that an oxidation reaction occurred during the interaction between the PS film and the laser (Figures S1–S3 and Table S1). A previous work[49] stated that the micropillar could grow with the heat accumulation by uninterrupted scanning due to the increase of the micropillar height and nanoparticles could not be sputtered inside the circle. During laser intermittent scanning, the produced

https://doi.org/10.1021/acsami.1c04049
ACS Appl. Mater. Interfaces 2021, 13, 23210–23219

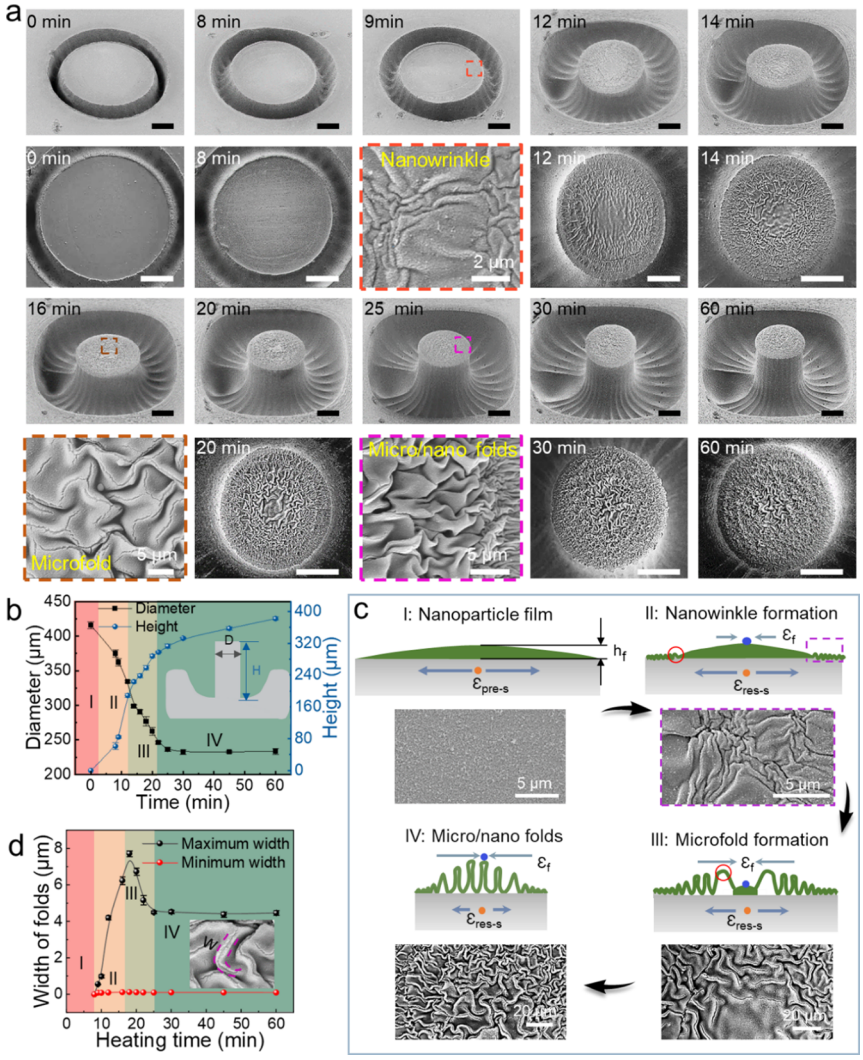

Figure 2. Evolution process and mechanism of 3D multiscale micro-/nanofolds. (a) Evolution process of the micropillar and its upper multiscale micro-/nanofolds for heating for 60 min. After heating for 9 min, the nanowrinkles emerge near the edge of the circle with the little shrinkage of the material. After heating for 16 min, the microfolds appear near the center of the circle with the medium shrinkage of the material. After heating for 25 min, the micropillar with the micro-/nanofolds are formed. The side view with a tilt angle of 45° and top view; scale bars: 100 μm. (b) Diameter and the height of the micropillar as the function of the heating time. (c) Formation mechanism of the multiscale micro-/nanofolds. Four stages of the multiscale micro-/nanofold formation. (I–IV) Nanoparticle film, nanowrinkle formation, microfold formation, and complete micro-/nanofolds. The SEM images show the corresponding microstructures. h_f, $\varepsilon_{pre\text{-}s}$, $\varepsilon_{res\text{-}s}$, and ε_f are the thickness of GTF, the prestrain of the substrate, the residue strain of the substrate, and the radial compressive strain acting on the nanoparticle GTF, respectively. With the decrease of $\varepsilon_{res\text{-}s}$, ε_f increases. The red circle indicates the front position of fold extension. (d) Maximum width and the minimum width of the micro-/nanofolds as the function of the heating time. The inset shows the site to measure the width of the micro-/nanofolds.

nanoparticles overlap in the center region, resulting in a GTF (left inset in Figure 1a). The microgrooves ablated by the laser and the resultant nanoparticles are shown in Figure 1c–f and Figure S4. Then, the SMP with the GTF is placed in the oven (115 °C) under the constrained heating condition for 25 min (if there are no constraints, the micropillars will be hidden in the substrate, Figure S4). Owing to the "self-growing effect,"[49] the material inside the circle shrinks and the micropillars are gradually formed (Figure 1b). During the heating process, the prestrain of the material ($\varepsilon_{pre\text{-}s}$) inside the circle is released, resulting in a radial compressive strain (ε_f) on the upper GTF. Interestingly, with the self-growth of the micropillar, the micro-/nanofolds are formed on the top simultaneously (right insets in Figure 1a,g–i), which is far different from the traditional two-dimensional shrinking-induced planar micro-/nanowrinkles.[27,36,38,52] It is noteworthy that the width of folds gradually increases from nanosize to microsize scales in the radial direction (Figure 1j).

2.2. Evolution Process and the Underlying Mechanism of 3D Multiscale Micro-/Nanofolds with Heating Time. To explore the physics of the process, the morphology evolution of 3D micro-/nanofolds with heating time is systematically investigated. Here, a circle with a diameter of 420 μm is scribed by laser for 40 times (only 2.3 s), and then heating is carried out for 60 min (Figure 2a). The SMP is heated above the targeted T_g for 9 min, where the material inside the circle begins to shrink, the upper GTF is subjected to ε_f, and the nanowrinkles emerge near the edge of the circle. Here, ε_f is calculated as $\varepsilon_f = (D_0 - D_a)/D_0$, where D_0 and D_a are the diameter of the micropillar before and after shrinkage, respectively. When heating it 16 min later, the material further shrinks, and the GTF near the center of the circle partially

https://doi.org/10.1021/acsami.1c04049
ACS Appl. Mater. Interfaces 2021, 13, 23210–23219

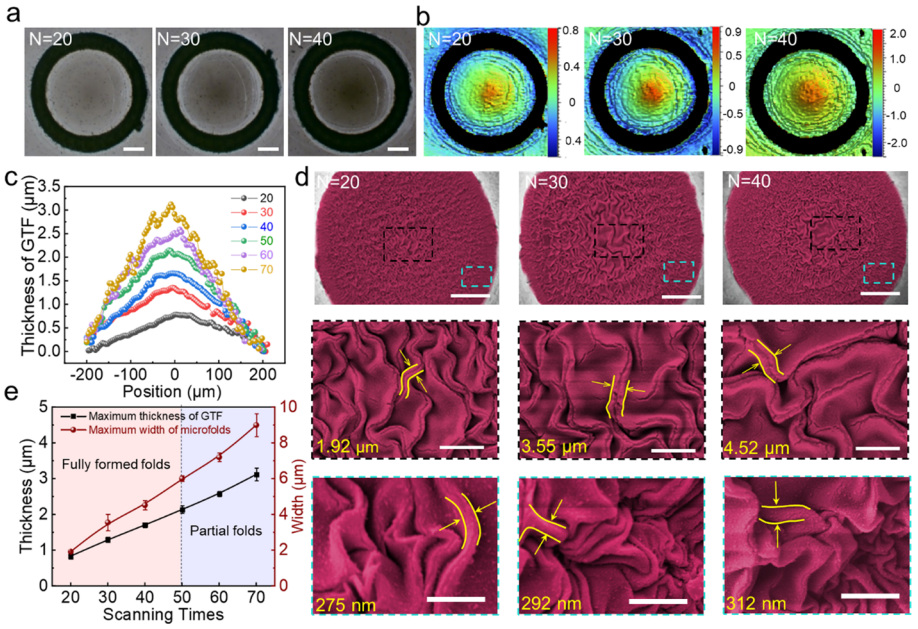

Figure 3. Controlling the multiscale micro-/nanofolds by varying the laser scanning times. (a) Optical images of the GTF inside the circle (diameter ~420 μm) which became darker with the increasing laser scanning numbers. Scale bars: 100 μm. (b) Corresponding 3D optical profile images of the GTF in (a). (c) Distribution of the nanoparticles in the radial direction at the different laser scanning times. The maximum thickness always lies in the center. (d) Pseudo-color SEM images show the corresponding morphology of multiscale micro- and nanofolds, respectively. Scale bars: 50 μm top row, 10 μm middle row, and 1 μm bottom row. (e) Maximum thickness of the GTF and the maximum width of formed microfolds as the function of the laser scanning times. When N is less than 50, the whole upper surface of the micropillar is covered by folds, while when N exceeds 50, the microfolds cannot be generated at the center.

detaches with the SMP; thus, the microfolds start to appear, while the central region remains flat. After heating for 25 min, the prestrain of the material is fully released, and the micro-/nanofolds cover the whole surface of the grown micropillar. After that, the micro-/nanofolds get stabilized. During heating, the diameter of the micropillar decreases from 420 μm ($\varepsilon_f = 0$) to 236 μm ($\varepsilon_f = 43.8\%$) and then remains unchanged (Figure 2b). Because the SMP is heated under the external constraints, the maximum ε_f (43.8%) is smaller than the shrinkage ratio of the SMP (55%). The height keeps increasing to 382 μm owing to the shrinkage of the material of the root.

According to the morphological characteristics of the microstructure, the formation of the multiscale micro-/nanofolds can be divided into four stages over heating time, which is schematically sketched in Figure 2c. In the first stage (heating for less than 9 min), the morphology of the GTF almost remains unchanged because heat accumulation is not enough to induce shrinkage of the material inside the circle. In the second stage (heating for 9−16 min), the nanowrinkles emerge near the edge of the circle. It is known that Young's modulus of the film E_f increases with the increase of film thickness h_f (Eq. 1),[53] and the critical stress to start wrinkling (σ_{crit}) also has a positive relationship with the E_f (Eq. 2)[20]

$$E_f \sim h_f \tag{1}$$

$$\sigma\text{crit} \sim \left(\frac{E_f}{1 - \nu_f^2}\right)^{1/3} \tag{2}$$

$$\lambda \sim h_f\left(\frac{E_f}{1 - \nu_f^2}\right)^{1/3} \tag{3}$$

where ν_f is Poisson's ratio of the nanoparticle GTF and regarded as the constant value. Within the elastic range, the principal compressive stress of the nanoparticle film (σ_f) is approximately equal to $E_f \times \varepsilon_f$. The thickness of the GTF in the central part (h_{fc}) is higher than that at its edge (h_{fe}); as a result, σ_f in this stage is larger than $\sigma_{crit,e}$ (the critical stress to start wrinkling of the edge), while it is smaller than $\sigma_{crit,c}$ (the critical stress to start wrinkling of the central region), and thus, the nanowrinkles emerge at the edge first. In the third stage (16−25 min), σ_f gradually increases to $\sigma_{crit,c}$ and the microfolds extend toward the center. At the end of this stage, the microfolds cover the whole central region. In the fourth stage (after 25 min), the formed micro-/nanofolds remain stable.

To systematically investigate the evolution of microstructures in the aforementioned four stages, the maximum and the minimum width are characterized as the feature sizes, as shown in Figure 2d. The width of the wrinkles (W, approximately equal to half the wavelength λ) has a positive relationship with h_f (Eq. 3);[15,21,54] thus, the maximum size structures always appear at the front position in the wrinkle extending direction (indicated with red circles in Figure 2c), and the maximum width increases to the peak value (9.2 μm) at 16 min (stage II). In the third stage, although the front position moves to a thicker site, σ_f is larger, and the microfolds are compressed and the maximum width decreases. In the fourth stage, the maximum width of microfolds remains stable at 4.5 μm. As for the minimum size structures, the width is the same for all stages (100 ± 30 nm).

2.3. Controllable Thickness of the GTF and the Corresponding 3D Multiscale Micro-/Nanofolds with Designed Laser Scanning Times. By virtue of the high precision processing capability of the femtosecond laser, the thickness of the GTF is accurately controlled by varying the

https://doi.org/10.1021/acsami.1c04049
ACS Appl. Mater. Interfaces 2021, 13, 23210−23219

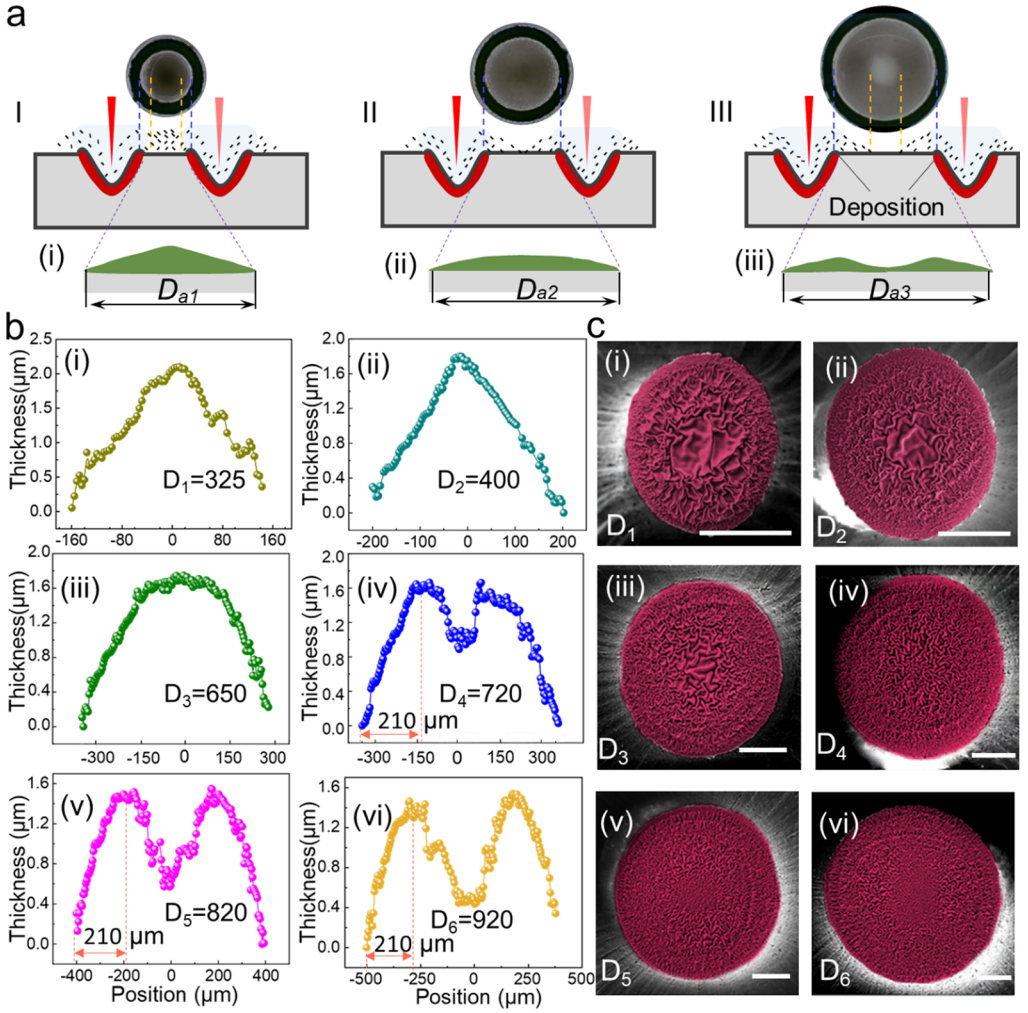

Figure 4. Controlling of the multiscale micro-/nanofolds by varying the diameters of the laser scanning path. (a) Schematic illustration of nanoparticle deposition at three different laser scanning paths: $D_{a1} < 2R_0$, $D_{a2} = 2R_0$, and $D_{a3} > 2R_0$. R_0 is about 325 μm, which is the distinguishable farthest distance of nanoparticles deposited when the laser scribes along the straight line. (b) Profiles of the GTF in the radial direction with increase of the diameters of the laser scanning path (from D_1 = 325 μm to D_6 = 920 μm). (c) Pseudo-color SEM images showing the corresponding morphology of the multiscale micro-/nanofolds. Scale bars: 100 μm.

laser scanning times (N). The optical images of the GTF inside the circle (diameter ~ 420 μm) with the increasing laser scanning times (from 20 to 70) are shown in Figure 3a and Figure S5. The color of the GTF is getting deeper in the radial direction, indicating that the nanoparticles generated by laser ablation have a gradient distribution. As the N increases, the color becomes darker owing to the further accumulation of the deposited nanoparticles. The 3D optical profile images also have a similar color change tendency (Figure 3b and Figure S5). The nanoparticles deposited along the radial direction show a Gaussian distribution, and the thickness of GTF increases with the laser scanning times (Figure 3c). After heating the SMP with the GTF, the formed multiscale micro-/nanofolds with different laser scanning times are shown in Figure 3d and Figures S5 and S6. When N is less than 10 (0.1 ~ 0.6 s), only the nanofolds are formed. When N is between 10 and 50, microfolds always appear at the center (larger h_f), and nanofolds locate in the edge of the circle (lower h_f). When N exceeds 50 (4 s at N = 70), the maximum thickness of the GTF is larger than the critical value (h_{fcrit}), leading to σ_f being smaller than the corresponding σ_{crit}, and the microfolds cannot be generated at the center. As shown in Figure 3e and Figures S6 and S7, the maximum thickness of the GTF increases linearly (from 830 nm to 3.12 μm) with the laser scanning times (from 20 to 70 scanning times), as well as the maximum width of the micro-/nanofolds (from 230 nm to 9.2 μm from 3 to 70 scanning times), which are well consistent with the wrinkling theory shown in Figure 2c.

2.4. Controllable Thickness of the GTF and the Corresponding 3D Multiscale Micro-/Nanofolds by the Laser Scanning Path. Furthermore, the laser scanning path with increasing diameters are varied to investigate the influence of the formation of the multiscale micro-/nanofolds. Prior to the experiment, it is found that the distinguishable farthest distance of nanoparticles deposited when the laser scribes along the straight line is about 325 μm (R_0, Figure S8) with the same laser power, scanning speed, and scanning times. Thus, three circles of different diameters, $D_{a1} < 2R_0$, $D_{a2} = 2R_0$, and $D_{a3} > 2R_0$, are employed to perform the experiment. Accordingly, the optical images of the generated GTFs are shown in Figure 4a. With regards to $D_{a1} < 2R_0$, the GTF is the darkest, owing to the accumulation of the nanoparticles in the center. As for $D_{a2} = 2R_0$, the GTF shows a uniform light black, indicating that the nanoparticles distribute homogenously near

https://doi.org/10.1021/acsami.1c04049
ACS Appl. Mater. Interfaces 2021, 13, 23210−23219

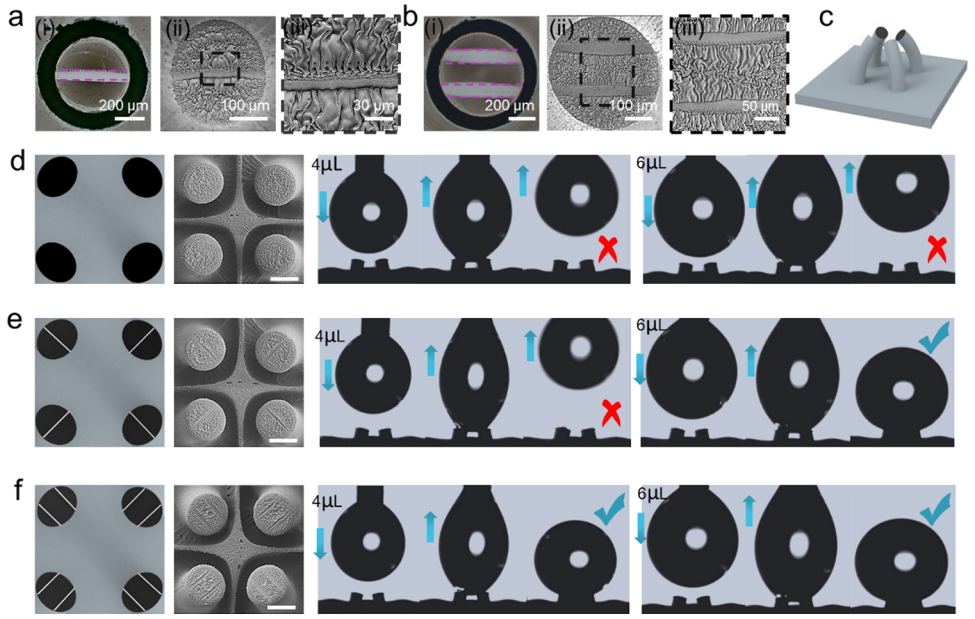

Figure 5. Template-free patterning of the micro-/nanofolds by laser cleaning and their tunable adhesion. (a) Patterned GTF can be easily obtained based on the laser cleaning effect. The nanoparticles distributed within the purple dotted lines are cleaned by in situ low power laser scanning. (i) Optical image of the single-line patterned GTF. (ii,iii) SEM images of the formed single-line patterned micro-/nanofolds. The orientation of micro-/nanofolds is perpendicular to the laser cleaning path. (b) Double-line patterned GTF and the corresponding micro-/nanofolds. (c) Schematic of the grown claw-like microstructure composed of four bent micropillars with micro-/nanofolds on the top. (d–f) Regulation of the adhesion by patterning the micro-/nanofolds. (d) Claw-like microstructure without patterned micro-/nanofolds on the top of each micropillar has a minimal adhesion and cannot pull the microdroplets (4 and 6 μL). (e) Claw-like microstructure with single-line patterned micro-/nanofolds on the top of each micropillar has a medium adhesion and can only pull 4 μL microdroplets. (f) Claw-like microstructure with double-lines patterned micro-/nanofolds on the top of each micropillar has the highest adhesion and can pull 4 and 6 μL microdroplets.

the center. While in terms of $D_{a3} > 2R_0$, the nanoparticles can hardly reach the center, giving rise to a clear circle region in the center. The 3D optical profile images show a similar color change tendency (Figure S9), and the nanoparticles distributed along the radial direction are quantitatively measured (Figure 4b). When $D_{a1} \leq 2R_0$ (D_1 = 325 μm, D_2 = 400 μm, and D_3 = 650 μm), the profile of the GTFs shows a Gaussian distribution (Figure 4b,i–iii), and the maximum thickness in the center decreases from 2.1 μm (D_1) to 1.71 μm (D_3). Correspondingly, the formed multiscale micro-/nanofolds when $D_{a1} \leq 2R_0$ are shown in Figure 4c,i–iii. Because the GTF maximum thicknesses of D_1 and D_2 are larger than the critical value (h_{fcrit}), the microfolds cannot be generated at the center. For D_3, the microfolds can cover the center, indicating that the maximum thickness of D_3 approaches to the h_{fcrit} (h_{fcrit} ~ 1.7 μm). In response to $D_{a3} > 2R_0$ (D_4 = 720 μm, D_5 = 820 μm, and D_6 = 920 μm), the profile of the GTFs shows an "M-like" distribution (Figure 4b,iv–vi), and the maximum thickness of the GTF decreases from 1.64 μm (D_4) to 1.45 μm (D_6). Interestingly, the peak values for the condition of $D_{a3} > 2R_0$ are always symmetrically located at about 210 μm away from the edge (Figure 4b). This may be the result of the combined effect of laser ablation-induced nanoparticle deposition and the subsequent laser cleaning. Accordingly, the formed multiscale micro-/nanofolds when $D_{a3} > 2R_0$ are shown in Figure 4c,iv–vi. The microstructures also show an "M-like" distribution along the radial direction, and nanofolds emerge around the center with a tendency to expand from D_4 to D_6.

2.5. Demonstration for Programmable Micro-/Nanofold Patterns and Tunable Adhesion. The patterned micro-/nanofolds have a wide range of applications in the tunable mechanical property,[37] metrology,[45,55] electronics,[56] and optics.[57−59] Here, by a template-free laser direct cleaning technique, the patterned GTF can be easily obtained (Figure 5a,b). When a femtosecond laser with a low-energy pulse irradiates the surface, it can produce a shockwave with a force high enough for nanoparticle removal at the laser fluence lower than damage threshold due to the high instantaneous peak power.[51] Combining the predesigned pattern, the nanoparticles are selectively cleaned. After heating, the formed single-line, double-line, and triangle-patterned micro-/nanofolds are shown in Figure 5a,b and Figure S10. The region cleaned by low power laser scanning shows the absence of micro-/nanofolds, while the other regions are covered by micro-/nanofolds with a perpendicular orientation to the laser cleaning path, owing to the boundary effect.[22,37] Based on our previously developed laser-induced polymer self-growing technique,[49] a claw-like microstructure composed of four bent micropillars with micro-/nanofolds on top of each is fabricated by one-time heating (Figure 5c), and then, the micropillars with micro-/nanofolds are treated with fluorosilane solution for improving the hydrophobicity. Owing to this special micro-/nanomorphology, the water/solid contact area is greatly reduced; thus, adhesion can be regulated. The claw-like microstructure with micro-/nanofolds on the whole top of each micropillar has a minimal adhesion and cannot pull the microdroplets (4 and 6 μL) (Figure 5d). For the claw-like microstructure with single-line patterned micro-/nanofolds on the top of each micropillar, the adhesion is medium, and the microstructure can only pull 4 μL microdroplets (Figure 5e). In regard to the claw-like microstructure with double-line patterned micro-/nanofolds on the top of each micropillar, the exposed region on the top of the micropillar is the largest; thus,

https://doi.org/10.1021/acsami.1c04049
ACS Appl. Mater. Interfaces 2021, 13, 23210−23219

the microstructure has the highest adhesion and can pull 4 and 6 μL microdroplets. The results demonstrate that the adhesion of the microstructure can be easily controlled by our presented method. To verify the mechanical stability and chemical durability of the formed 3D multiscale micro-/nanofolds, the microstructures are ultrasonically cleaned for 1 h in water and immersed in it and HCl and NaOH solutions for 4 days. As displayed in Figure S11, the microstructures remain intact, demonstrating the robustness of these micro-/nanostructures.

3. CONCLUSIONS

In summary, we propose a rapid, facile, and highly controllable method for realizing robust 3D multiscale hierarchical micro-/nanofolds. By laser intermittent ablation on the SMP, the nanoparticle film with gradient thickness is quickly and facilely obtained (100 ms−4 s). Following one-time constrained heating, the 3D micropillars grow out of the substrate, and the nanoparticle gradient film on its top shrinks into multiscale micro-/nanofolds simultaneously. The underlying mechanism is revealed by systematically investigating the evolution process of the 3D micro-/nanofolds. Based on this, the thickness of the gradient film and the feature size of the formed micro-/nanofolds are accurately controlled by regulating the laser scanning path and scanning times. Furthermore, relying on the advantage of laser cleaning technology, noncontact and template-free patterning of the micro-/nanofolds is realized, and the hierarchically structured surfaces with tunable adhesion to the water droplet are demonstrated. The method combining the superior deformability of the SMP film and femtosecond laser high precision processing capability opens up a new avenue to prepare the GTF and functional microstructures with great scalability and flexibility toward promising applications.

4. EXPERIMENTAL SECTION

4.1. Fabrication and Heating. The SMP film (PS film) of 0.15 mm thickness is purchased from Dongguan Nogard Arts & Crafts Factory. AutoCAD 2019 was utilized to design the pattern of circles in the film. Then, the CAD file was imported to the processing software (Samlight) to guide laser scanning. The laser beam (104 fs, 1 kHz, 800 nm) from a regenerative amplified Ti: sapphire femtosecond laser system (Legend Elite-1 K-HE, Coherent, USA) was employed for ablation. During the fabrication process, laser beam was guided onto the SMP surface by a galvanometric system (SCANLAB, Germany) equipped with a telecentric *f*-theta lens with a focal length of 63 mm. The laser power was adjusted to 250 mw, and the scanning speed was 50 mm/s. The scanning times were controlled by the software Samlight. After processing, the periphery of the SMP film with circle arrays was fixed by iron clamps. Finally, the sample was placed in an oven and heated at 115 °C. The preparation of the pattern was followed by in situ defocus scanning on the as-prepared GTF. The power was about 9 mw, which was adjusted by combining a half-wave plate and a low dispersion polarizer, speed was 15 mm/s, and scanning times was 1.

4.2. Adhesion and Robustness Experiment. First, fluorosilane (1H, 1H, 2H, and 2H-perfluorodecyltriethoxysilane) was mixed with ethanol with a mass ratio of 1:85 at room temperature, and then, the mixed solution was thoroughly stirred. The three different claw-like microstructures with patterned micro-/nanofolds on the top of micropillars (no-patterned, single-line, and double-line) were immersed in fluorosilane solution for 12 h to improve their hydrophobicity. Then, they were fixed on the CA100C (Shanghai Innuo Precision Instruments Co., Ltd., Shanghai, China), droplets (4 and 6 μL) were extruded through a syringe, then slowly touches the upper surface of claw-like in the vertical direction, and slowly lifted. In addition, the 3D multiscale micro-/nanofolds were immersed in HCl (1 mol L^{-1}), NaOH (1 mol L^{-1}) solutions and water for 4 days.

4.3. Characterization. The SEM images were taken with a secondary electron scanning electron microscope (ZEISS EVO18) operated at an accelerating voltage of 10 keV after the samples were sputter-coated with gold for 120 s. An optical microscope (LW200-3JT) was used to observe the top view of the GTF. Three-dimensional profile images were obtained by a 3D Optical Profiler (Contour GT-K, Bruker Company, Germany).

■ ASSOCIATED CONTENT

Supporting Information

The Supporting Information is available free of charge at https://pubs.acs.org/doi/10.1021/acsami.1c04049.

EDS analysis of the PS film and nanoparticles, FT-IR characterization of PS and nanoparticles, XPS analysis of the PS film and nanoparticles, microgrooves and the nanoparticles, the morphology and feature size of micro-/nanofolds with different laser scanning times, the width of the micro-/nanofolds as the function of the scanning times, distinguishable farthest distance of nanoparticles deposited, 3D optical profile images with different laser scanning diameters, triangle-patterned micro-/nanofolds, and robustness of the 3D multiscale micro-/nanofolds (PDF)

■ AUTHOR INFORMATION

Corresponding Authors

Jiawen Li − *CAS Key Laboratory of Mechanical Behavior and Design of Materials, Key Laboratory of Precision Scientific Instrumentation of Anhui Higher Education Institutes, Department of Precision Machinery and Precision Instrumentation, University of Science and Technology of China, Hefei, Anhui 230027, China;* orcid.org/0000-0003-3950-6212; Email: jwl@ustc.edu.cn

Dong Wu − *CAS Key Laboratory of Mechanical Behavior and Design of Materials, Key Laboratory of Precision Scientific Instrumentation of Anhui Higher Education Institutes, Department of Precision Machinery and Precision Instrumentation, University of Science and Technology of China, Hefei, Anhui 230027, China;* orcid.org/0000-0003-0623-1515; Email: dongwu@ustc.edu.cn

Authors

Cheng Xue − *CAS Key Laboratory of Mechanical Behavior and Design of Materials, Key Laboratory of Precision Scientific Instrumentation of Anhui Higher Education Institutes, Department of Precision Machinery and Precision Instrumentation, University of Science and Technology of China, Hefei, Anhui 230027, China*

Yachao Zhang − *CAS Key Laboratory of Mechanical Behavior and Design of Materials, Key Laboratory of Precision Scientific Instrumentation of Anhui Higher Education Institutes, Department of Precision Machinery and Precision Instrumentation, University of Science and Technology of China, Hefei, Anhui 230027, China*

Longfu Li − *CAS Key Laboratory of Mechanical Behavior and Design of Materials, Key Laboratory of Precision Scientific Instrumentation of Anhui Higher Education Institutes, Department of Precision Machinery and Precision Instrumentation, University of Science and Technology of China, Hefei, Anhui 230027, China*

Yanlei Hu − *CAS Key Laboratory of Mechanical Behavior and Design of Materials, Key Laboratory of Precision Scientific Instrumentation of Anhui Higher Education Institutes, Department of Precision Machinery and Precision Instrumentation, University of Science and Technology of China, Hefei, Anhui 230027, China;* orcid.org/0000-0003-1964-0043

Chao Chen − *CAS Key Laboratory of Mechanical Behavior and Design of Materials, Key Laboratory of Precision Scientific Instrumentation of Anhui Higher Education Institutes, Department of Precision Machinery and Precision Instrumentation, University of Science and Technology of China, Hefei, Anhui 230027, China*

Yuegan Song − *CAS Key Laboratory of Mechanical Behavior and Design of Materials, Key Laboratory of Precision Scientific Instrumentation of Anhui Higher Education Institutes, Department of Precision Machinery and Precision Instrumentation, University of Science and Technology of China, Hefei, Anhui 230027, China*

Hongshu You − *CAS Key Laboratory of Mechanical Behavior and Design of Materials, Key Laboratory of Precision Scientific Instrumentation of Anhui Higher Education Institutes, Department of Precision Machinery and Precision Instrumentation, University of Science and Technology of China, Hefei, Anhui 230027, China*

Rui Li − *CAS Key Laboratory of Mechanical Behavior and Design of Materials, Key Laboratory of Precision Scientific Instrumentation of Anhui Higher Education Institutes, Department of Precision Machinery and Precision Instrumentation, University of Science and Technology of China, Hefei, Anhui 230027, China*

Jiaru Chu − *CAS Key Laboratory of Mechanical Behavior and Design of Materials, Key Laboratory of Precision Scientific Instrumentation of Anhui Higher Education Institutes, Department of Precision Machinery and Precision Instrumentation, University of Science and Technology of China, Hefei, Anhui 230027, China;* orcid.org/0000-0001-6472-8103

Complete contact information is available at: https://pubs.acs.org/10.1021/acsami.1c04049

Author Contributions

C.X. and Y.Z. designed the experiment. C.X., L.L., and H.Y. fabricated samples. C.X., Y.Z., Y.S., and R.L. took pictures. C.X. and L.L. performed the adhesion and robustness experiment. C.X., Y.Z., and Y.H. analyzed the data and prepared the manuscript. D.W., J.L., C.C., and J.C. reviewed and revised the article. C.X. and Y.Z. contributed equally to this work.

Notes

The authors declare no competing financial interest.

■ ACKNOWLEDGMENTS

This work was supported by the National Key R&D Program of China (2017YFB1104303 and 2018YFB1105400), National Natural Science Foundation of China (61927814, 91963127, 51875544, 51805509, 52075516, and 62005262), Major Scientific and Technological Projects in Anhui Province (201903a05020005), the Fundamental Research Funds for the Central Universities (YD2090002005 and WK 5290000001), and Youth Innovation Promotion Association CAS (2017495). The authors acknowledge the Experimental Center of Engineering and Material Sciences at USTC for the fabrication and measuring of samples. This work was partly carried out at the USTC Center for Micro and Nanoscale Research and Fabrication.

■ REFERENCES

(1) Geim, A. K.; Dubonos, S. V.; Grigorieva, I. V.; Novoselov, K. S.; Zhukov, A. A.; Shapoval, S. Y. Microfabricated Adhesive Mimicking Gecko Foot-Hair. *Nat. Mater.* **2003**, *2*, 461−463.

(2) Lee, H.; Lee, B. P.; Messersmith, P. B. A reversible Wet/Dry Adhesive Inspired by Mussels and Geckos. *Nature* **2007**, *448*, 338−341.

(3) Barthlott, W.; Neinhuis, C. Purity of the Sacred Lotus, or Escape from Contamination in Biological Surfaces. *Planta* **1997**, *202*, 1−8.

(4) Jiang, L.; Zhao, Y.; Zhai, J. A Lotus-Leaf-like Superhydrophobic Surface: A Porous Microsphere/Nanofiber Composite Film Prepared by Electrohydrodynamics. *Angew. Chem., Int. Ed.* **2004**, *43*, 4338−4341.

(5) Koch, K.; Bhushan, B.; Jung, Y. C.; Barthlott, W. Fabrication of Artificial Lotus Leaves and Significance of Hierarchical Structure for Superhydrophobicity and Low Adhesion. *Soft Matter* **2009**, *5*, 1386−1393.

(6) Gao, X.; Yan, X.; Yao, X.; Xu, L.; Zhang, K.; Zhang, J.; Yang, B.; Jiang, L. The Dry-Style Antifogging Properties of Mosquito Compound Eyes and Artificial Analogues Prepared by Soft Lithography. *Adv. Mater.* **2007**, *19*, 2213−2217.

(7) Li, J.; Wang, W.; Mei, X.; Pan, A.; Sun, X.; Liu, B.; Cui, J. Artificial Compound Eyes Prepared by a Combination of Air-Assisted Deformation, Modified Laser Swelling, and Controlled Crystal Growth. *ACS Nano* **2019**, *13*, 114−124.

(8) Audrey, Y. Y. H.; Lip, P. Y.; Yee, C. L.; Isabel, R. Fabrication and Analysis of Gecko-Inspired Hierarchical Polymer Nanosetae. *ACS Nano* **2011**, *5*, 1897−1906.

(9) Chen, H.; Ran, T.; Gan, Y.; Zhou, J.; Zhang, Y.; Zhang, L.; Zhang, D.; Jiang, L. Ultrafast Water Harvesting and Transport in Hierarchical Microchannels. *Nat. Mater.* **2018**, *17*, 935−942.

(10) Chen, H.; Zhang, P.; Zhang, L.; Liu, H.; Jiang, Y.; Zhang, D.; Han, Z.; Jiang, L. Continuous Directional Water Transport on the Peristome Surface of Nepenthes Alata. *Nature* **2016**, *532*, 85−89.

(11) Jiang, H.-B.; Zhang, Y. L.; Liu, Y.; Fu, X. Y.; Li, Y. F.; Liu, Y. Q.; Li, C.-H.; Sun, H. B. Bioinspired Few-Layer Graphene Prepared by Chemical Vapor Deposition on Femtosecond Laser-Structured Cu foil. *Laser Photonics Rev.* **2016**, *10*, 441−450.

(12) Zhang, L.; Sun, L.; Zhang, Z.; Wang, Y.; Yang, Z.; Liu, C.; Li, Z.; Zhao, Y. Bioinspired Superhydrophobic Surface by Hierarchically Colloidal Assembling of Microparticles and Colloidal Nanoparticles. *Chem. Eng. J.* **2020**, *394*, No. 125008.

(13) Zheng, Y.; Bai, H.; Huang, Z.; Tian, X.; Nie, F.-Q.; Zhao, Y.; Zhai, J.; Jiang, L. Directional Water Collection on Wetted Spider Silk. *Nature* **2010**, *463*, 640−643.

(14) Bae, W. G.; Kim, H. N.; Kim, D.; Park, S. H.; Jeong, H. E.; Suh, K. Y. 25th Anniversary Article: Scalable Multiscale Patterned Structures Inspired by Nature: The Role of Hierarchy. *Adv. Mater.* **2014**, *26*, 675−700.

(15) Chen, X.; Yin, J. Buckling Patterns of Thin Films on Curved Compliant Substrates with Applications to Morphogenesis and Three-Dimensional Micro-Fabrication. *Soft Matter* **2010**, *6*, 5667−5680.

(16) Lee, W.-K.; Engel, C. J.; Huntington, M. D.; Hu, J.; Odom, T. W. Controlled Three-Dimensional Hierarchical Structuring by Memory-Based, Sequential Wrinkling. *Nano Lett.* **2015**, *15*, 5624−5629.

(17) Mu, J.; Hou, C.; Wang, G.; Wang, X.; Zhang, Q.; Li, Y.; Wang, H.; Zhu, M. An Elastic Transparent Conductor Based on Hierarchically Wrinkled Reduced Graphene Oxide for Artificial Muscles and Sensors. *Adv. Mater.* **2016**, *28*, 9491−9497.

(18) Rahmawan, Y.; Moon, M.-W.; Kim, K.-S.; Lee, K.-R.; Suh, K.-Y. Wrinkled, Dual-Scale Structures of Diamond-Like Carbon (DLC) for Superhydrophobicity. *Langmuir* **2010**, *26*, 484−491.

(19) Tan, Y.; Hu, B.; Song, J.; Chu, Z.; Wu, W. Bioinspired Multiscale Wrinkling Patterns on Curved Substrates: An Overview. *Nano-Micro Lett.* **2020**, *12*, 101.
(20) Bowden, N.; Brittain, S.; Evans, A.; Hutchinson, J.; Whitesides, G. Spontaneous Formation of Ordered Structures in Thin Films of Metals Supported on an Elastomeric Polymer. *Nature* **1998**, *393*, 146−149.
(21) Chung, J. Y.; Nolte, A. J.; Stafford, C. M. Surface Wrinkling: A Versatile Platform for Measuring Thin-Film Properties. *Adv. Mater.* **2011**, *23*, 349−368.
(22) Ding, W.; Yang, Y.; Zhao, Y.; Jiang, S.; Cao, Y.; Lu, C. Well-defined Orthogonal Surface Wrinkles Directed by the Wrinkled Boundary. *Soft Matter* **2013**, *9*, 3720−3726.
(23) Li, B.; Cao, Y.-P.; Feng, X.-Q.; Gao, H. Mechanics of Morphological Instabilities and Surface Wrinkling in Soft Materials: A Review. *Soft Matter* **2012**, *8*, 5728−5745.
(24) Rhee, D.; Deng, S.; Odom, T. W. Soft Skin Layers for Reconfigurable and Programmable Nanowrinkles. *Nanoscale* **2020**, *12*, 23920−23928.
(25) Yang, X.; Zhao, Y.; Xie, J.; Han, X.; Wang, J.; Zong, C.; Ji, H.; Zhao, J.; Jiang, S.; Cao, Y.; Lu, C. Bioinspired Fabrication of Free-Standing Conducting Films with Hierarchical Surface Wrinkling Patterns. *ACS Nano* **2016**, *10*, 3801−3808.
(26) Cao, C.; Chan, H. F.; Zang, J.; Leong, K. W.; Zhao, X. Harnessing Localized Ridges for High-Aspect-Ratio Hierarchical Patterns with Dynamic Tunability and Multifunctionality. *Adv. Mater.* **2014**, *26*, 1763−1770.
(27) Fu, C.-C.; Grimes, A.; Long, M.; Ferri, C. G. L.; Rich, B. D.; Ghosh, S.; Ghosh, S.; Lee, L. P.; Gopinathan, A.; Khine, M. Tunable Nanowrinkles on Shape Memory Polymer Sheets. *Adv. Mater.* **2009**, *21*, 4472−4476.
(28) Yuan, H.; Wu, K.; Zhang, J.; Wang, Y.; Liu, G.; Sun, J. Curvature-Controlled Wrinkling Surfaces for Friction. *Adv. Mater.* **2019**, *31*, No. 1900933.
(29) Takei, A.; Jin, L.; Fujita, H.; Takei, A.; Fujita, H.; Jin, L. High-Aspect-Ratio Ridge Structures Induced by Plastic Deformation as a Novel Microfabrication Technique. *ACS Appl. Mater. Interfaces* **2016**, *8*, 24230−24237.
(30) Tan, Y.; Yan, J.; Chu, Z. Thermal-Shrinking-Induced Ring-Patterned Boron Nitride Wrinkles on Carbon Fibers. *Carbon* **2019**, *152*, 532−536.
(31) Hou, H.; Yin, J.; Jiang, X. Reversible Diels-Alder Reaction to Control Wrinkle Patterns: From Dynamic Chemistry to Dynamic Patterns. *Adv. Mater.* **2016**, *28*, 9126−9132.
(32) Ma, T.; Li, T.; Zhou, L.; Ma, X.; Yin, J.; Jiang, X. Dynamic Wrinkling Pattern Exhibiting Tunable Fluorescence for Anticounterfeiting Applications. *Nat. Commun.* **2020**, *11*, 1811−1818.
(33) Troy, R. H.; Ilsoon, L. Wrinkle-Free Nanomechanical Film: Control and Prevention of Polymer Film Buckling. *Nano Lett.* **2007**, *7*, 372−379.
(34) Evensen, H. T.; Jiang, H.; Gotrik, K. W.; Denes, F.; Carpick, R. W. Transformations in Wrinkle Patterns: Cooperation between Nanoscale Cross-Linked Surface Layers and the Submicrometer Bulk in Wafer-Spun, Plasma-Treated Polydimethylsiloxane. *Nano Lett.* **2009**, *9*, 2884−2890.
(35) Li, Q.; Han, X.; Hou, J.; Yin, J.; Jiang, S.; Lu, C. Patterning Poly(dimethylsiloxane) Microspheres via Combination of Oxygen Plasma Exposure and Solvent Treatment. *J. Phys. Chem. B* **2015**, *119*, 13450−13461.
(36) Huntington, M. D.; Engel, C. J.; Hryn, A. J.; Odom, T. W. Polymer Nanowrinkles with Continuously Tunable Wavelengths. *ACS Appl. Mater. Interfaces* **2013**, *5*, 6438−6442.
(37) Lee, W. K.; Kang, J.; Chen, K. S.; Engel, C. J.; Jung, W. B.; Rhee, D.; Hersam, M. C.; Odom, T. W. Multiscale, Hierarchical Patterning of Graphene by Conformal Wrinkling. *Nano Lett.* **2016**, *16*, 7121−7127.
(38) Lee, W.-K.; Jung, W.-B.; Rhee, D.; Hu, J.; Lee, Y.-A. L.; Jacobson, C.; Jung, H.-T.; Odom, T. W. Monolithic Polymer Nanoridges with Programmable Wetting Transitions. *Adv. Mater.* **2018**, *30*, No. 1706657.
(39) Chandra, D.; Yang, S.; Lin, P. C. Strain Responsive Concave and Convex Microlens Arrays. *Appl. Phys. Lett.* **2007**, *91*, No. 251912.
(40) Chung, J. Y.; Nolte, A. J.; Stafford, C. M. Diffusion-Controlled, Self-Organized Growth of Symmetric Wrinkling Patterns. *Adv. Mater.* **2009**, *21*, 1358−1362.
(41) Gao, N.; Zhang, X.; Liao, S.; Jia, H.; Wang, Y. Polymer Swelling Induced Conductive Wrinkles for an Ultrasensitive Pressure Sensor. *ACS Macro Lett.* **2016**, *5*, 823−827.
(42) Li, M.; Hakimi, N.; Perez, R.; Waldman, S.; Kozinski, J. A.; Hwang, D. K. Microarchitecture for a Three-Dimensional Wrinkled Surface Platform. *Adv. Mater.* **2015**, *27*, 1880−1886.
(43) Song, J.; Tan, Y.; Chu, Z.; Xiao, M.; Li, G.; Jiang, Z.; Wang, J.; Hu, T. Hierarchical Reduced Graphene Oxide Ridges for Stretchable, Wearable, and Washable Strain Sensors. *ACS Appl. Mater. Interfaces* **2019**, *11*, 1283−1293.
(44) Tan, Y.; Chu, Z.; Jiang, Z.; Hu, T.; Li, G.; Song, J. Gyrification-Inspired Highly Convoluted Graphene Oxide Patterns for Ultralarge Deforming Actuators. *ACS Nano* **2017**, *11*, 6843−6852.
(45) Stafford, C. M.; Harrison, C.; Beers, K. L.; Karim, A.; Amis, E. J.; VanLandingham, M. R.; Kim, H. C.; Volksen, W.; Miller, R. D.; Simonyi, E. E. A Buckling-Based Metrology for Measuring the Elastic Moduli of Polymeric Thin Films. *Nat. Mater.* **2004**, *3*, 545−550.
(46) Stafford, C. M.; Roskov, K. E.; Epps, T. H.; Fasolka, M. J. Generating Thickness Gradients of Thin Polymer Films Via Flow Coating. *Rev. Sci. Instrum.* **2006**, *77*, No. 023908.
(47) Tan, Y.; Hu, B.; Chu, Z.; Wu, W. Bioinspired Superhydrophobic Papillae with Tunable Adhesive Force and Ultralarge Liquid Capacity for Microdroplet Manipulation. *Adv. Func. Mater.* **2019**, *29*, No. 1900266.
(48) Yu, S.; Ni, Y.; He, L.; Ye, Q. L. Tunable Formation of Ordered Wrinkles in Metal Films with Controlled Thickness Gradients Deposited on Soft Elastic Substrates. *ACS Appl. Mater. Interfaces* **2015**, *7*, 5160−5167.
(49) Zhang, Y.; Li, Y.; Hu, Y.; Zhu, X.; Huang, Y.; Zhang, Z.; Rao, S.; Hu, Z.; Qiu, W.; Wang, Y.; Li, G.; Yang, L.; Li, J.; Wu, D.; Huang, W.; Qiu, C.; Chu, J. Localized Self-Growth of Reconfigurable Architectures Induced by a Femtosecond Laser on a Shape-Memory Polymer. *Adv. Mater.* **2018**, *30*, No. 1803072.
(50) Chen, T.; Wang, W.; Tao, T.; Pan, A.; Mei, X. Multi-Scale Micro-Nano Structures Prepared by Laser Cleaning Assisted Laser Ablation for Broadband Ultralow Reflectivity Silicon Surfaces in Ambient air. *Appl. Surf. Sci.* **2020**, *509*, No. 145182.
(51) Park, J.-K.; Yoon, J.-W.; Cho, S. H. Removal of Nanoparticles from A Silicon Wafer Using Plasma Shockwaves Excited with A Femtosecond Laser. *Appl. Surf. Sci.* **2012**, *258*, 6379−6383.
(52) Zang, J.; Ryu, S.; Pugno, N.; Wang, Q.; Tu, Q.; Buehler, M. J.; Zhao, X. Multifunctionality and Control of the Crumpling and Unfolding of Large-Area Graphene. *Nat. Mater.* **2013**, *12*, 321−325.
(53) Yin, J.; Chen, X. Elastic Buckling of Gradient Thin Films on Compliant Substrates. *Philos. Mag. Lett.* **2010**, *90*, 423−433.
(54) Genzer, J.; Groenewold, J. Soft Matter with Hard Skin: From Skin Wrinkles to Templating and Material Characterization. *Soft Matter* **2006**, *2*, 310−323.
(55) Lee, J. H.; Ro, H. W.; Huang, R.; Lemaillet, P.; Germer, T. A.; Soles, C. L.; Stafford, C. M. Anisotropic, Hierarchical Surface Patterns Via Surface Wrinkling of Nanopatterned Polymer Films. *Nano Lett.* **2012**, *12*, 5995−5999.
(56) Chae, S. H.; Yu, W. J.; Bae, J. J.; Duong, D. L.; Perello, D.; Jeong, H. Y.; Ta, Q. H.; Ly, T. H.; Vu, Q. A.; Yun, M.; Duan, X.; Lee, Y. H. Transferred Wrinkled Al2O3 for Highly Stretchable and Transparent Graphene−Carbon Nanotube Transistors. *Nat. Mater.* **2013**, *12*, 403−409.
(57) Li, F. D.; Hou, H. H.; Yin, J.; Jiang, X. S. Near-Infrared Light−Responsive Dynamic Wrinkle Patterns. *Sci. Adv.* **2018**, *4*, No. eaar5762.
(58) Lee, E.; Zhang, M.; Cho, Y.; Cui, Y.; Van der Spiegel, J.; Engheta, N.; Yang, S. Tilted Pillars on Wrinkled Elastomers as A

Reversibly Tunable Optical Window. *Adv. Mater.* **2014**, *26*, 4127−4133.
(59) Wang, J.; Xie, J.; Zong, C.; Han, X.; Zhao, J.; Jiang, S.; Cao, Y.; Fery, A.; Lu, C. Light-Modulated Surface Micropatterns with Multifunctional Surface Properties on Photodegradable Polymer Films. *ACS Appl. Mater. Interfaces* **2017**, *9*, 37402−37410.

https://doi.org/10.1021/acsami.1c04049
ACS Appl. Mater. Interfaces 2021, 13, 23210−23219